

# Color Variants Identification in Fashion e-commerce via Contrastive Self-Supervised Representation Learning

Ujjal Kr Dutta , Sandeep Repakula , Maulik Parmar and Abhinav Ravi

Data Sciences-Image Sciences, Myntra  
Bengaluru, Karnataka, India

{ujjal.dutta,sandeep.r,parmar.m,abhinav.ravi}@myntra.com

## Abstract

In this paper, we utilize deep visual Representation Learning to address an important problem in fashion e-commerce: color variants identification, i.e., identifying fashion products that match exactly in their design (or style), but only to differ in their color. At first we attempt to tackle the problem by obtaining manual annotations (depicting whether two products are color variants), and train a supervised triplet loss based neural network model to learn representations of fashion products. However, for large scale real-world industrial datasets such as addressed in our paper, it is infeasible to obtain annotations for the entire dataset, while capturing all the difficult corner cases. Interestingly, we observed that color variants are essentially manifestations of color jitter based augmentations. Thus, we instead explore Self-Supervised Learning (SSL) to solve this problem. We observed that existing state-of-the-art SSL methods perform poor, for our problem. To address this, we propose a novel SSL based color variants model that simultaneously focuses on different parts of an apparel. Quantitative and qualitative evaluation shows that our method outperforms existing SSL methods, and at times, the supervised model.

## 1 Introduction

In this paper, we address a very crucial problem in fashion e-commerce, namely, automated *color variants identification*, i.e., identifying fashion products that match exactly in their design (or style), but only to differ in their color (Figure 1). Our motivation to pick the use-case of color variants identification for fashion products comes from the following reasons: i) Fashion products top across all categories in online retail sales [Jagadeesh *et al.*, 2014], ii) Most often users hesitate to buy a fashion product solely due to its color despite liking all other aspects of it. Providing more color options increases add-to-cart ratio, thereby generating more revenue, along with improved customer experience. At Myntra (www.myntra.com), a leading e-commerce platform, we address this problem by leveraging deep visual Representation/Embedding Learning.

Firstly, we obtained manual annotations (class labels) indicating whether two product images are color variants to



Figure 1: Illustration of the *color variants identification* problem. The anchor and positive images contain fashion products that have the exact same design/ style, but different colors (anchor is blue, and positive is black). The negative image contains a product that is not a color variant to the anchor and the positive. NOTE: The images belong to www.myntra.com.

each other. These class labels are used to obtain triplet based constraints, consisting of an anchor, a positive and a negative (Figure 1). The positive is usually an image that consists of a product that is a color variant of the product contained in the anchor image. The negative is an image that consists of a product that is not a color variant of the products contained in the anchor and positive images. These triplets are used to train a supervised triplet loss based neural network model [Schroff *et al.*, 2015; Veit *et al.*, 2017] in order to obtain deep embeddings of fashion products. Having obtained the embeddings, we perform clustering on them to group the color variants.

A key challenge in this supervised approach is that of obtaining manual annotations, which not only requires fashion domain expertise, but is also infeasible, given the large scale of our platform, and the huge number and complexity of the fashion products. As visual Self-Supervised Learning (SSL) obtains image embeddings without requiring manual annotations, we consider it as a candidate to address our problem, i.e., lack of annotations for our large data. The motivation for this comes from the fact that typical visual SSL methods employ a color jitter based data augmentation step.

Interestingly, color variants of fashion products are in essence, manifestations of color jittering. It should be noted that a Product Display Page (PDP) image in a fashion e-commerce platform may contain multiple fashion products. Thus, we must apply an object detector to localise our primary fashion product of interest (Figure 3). However, when we already employ object detection, the standard random crop step used in existing SSL methods may actually miss out im-

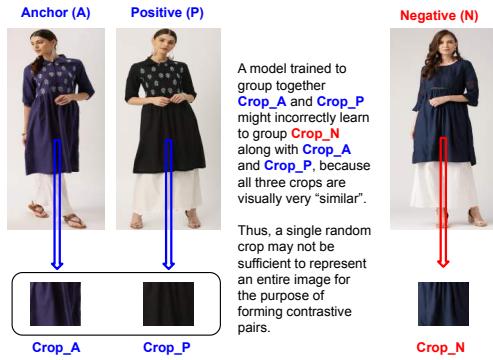


Figure 2: Drawbacks of using random crop to form contrastive pairs in our use-case.

portant regions of a fashion product, which might be crucial in identifying color variants (Figure 2).

For this reason, we rather choose to propose a novel SSL variation that considers multiple slices/ patches of the primary fashion object (after object detection), and simultaneously obtains embeddings for each of them. The final sum-pooled embedding is then used to optimize a SSL based contrastive loss (Figure 4). We call our method as **Patch-Based Contrastive Net (PBCNet)**. We conjecture that considering multiple patches i) do not leave things to chance (as in random crops), and provides a deterministic approach to obtain embeddings, ii) enables us to borrow more information (from other patches) to make a better decision on grouping a pair of similar embeddings. Our conjecture is supported not only by evidence of improved discriminative performances by the consideration of multiple fine patches of images [Wang *et al.*, 2018], but also by our experimental results, where our method consistently outperforms existing SSL methods on our task, and also the supervised baseline.

Following are the **major contributions of the paper**:

1. A supervised triplet loss based visual Representation Learning approach to identify color variants among fashion products (to the best of our knowledge addressed for the first time).
2. A systematic study of existing state-of-the-art SSL methods to solve the proposed problem while alleviating the need for manual annotations.
3. A novel contrastive loss based SSL method that focuses on parts of an object to identify color variants.

## 2 Related Work

The problem of visual embedding/ metric learning refers to that of obtaining vector representations/embeddings of images in a way that the embeddings of similar images are grouped together while moving away dissimilar ones. Several approaches have been proposed in the recent literature, which can be categorized as either supervised [Sun *et al.*, 2020; Levi *et al.*, 2020; Gu and Ko, 2020] or unsupervised [Dutta *et al.*, 2020b; Cao *et al.*, 2019; Li *et al.*, 2020; Dutta *et al.*, 2020a]. Typically, a key aspect of such approaches is that of providing constraints for optimizing a suitable objective function. Popular forms of constraints in embedding learning are either in the form of pairs, triplets or tuples, that indicate embeddings of which examples need to be brought closer.

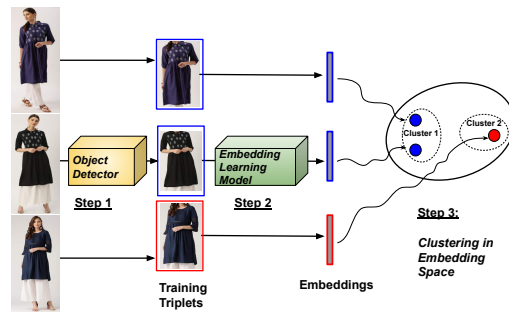


Figure 3: Proposed pipeline to address the color variants identification problem by using a supervised embedding learning model.

Visual SSL [Jing and Tian, 2020] refers to the learning of representations of images without making use of class labels. A popular paradigm of SSL is contrastive learning, that groups together embeddings obtained from augmentations of the same image. Many recent SSL approaches have been proposed that vary in their implementation details (for example, using momentum encoding, memory module, only positive pairs, etc) [Chen *et al.*, 2020; He *et al.*, 2020; Grill *et al.*, 2020; Chen and He, 2021].

## 3 Proposed Approach

In this section, we discuss the Representation Learning methods used to address the problem of color variants identification.

### 3.1 Supervised Color Variants Model

Firstly, we shall discuss the proposed supervised approach of addressing the color variants identification problem. Our proposed pipeline leveraging the supervised model is illustrated in Figure 3. The pipeline consists of the following major components (or steps) in the same order: i) Object Detection, ii) Embedding Learning and iii) Clustering. As the original input image usually consists of a human model wearing secondary fashion products as well, we perform object detection to localise the primary fashion product of interest. Having obtained the cropped image of the fashion article, we form triplet based constraints (in the form of anchor, positive and negative) using the available manual annotations. These triplets are used to train an embedding learning model. The obtained embeddings are then grouped together by using an appropriate clustering algorithm. An obtained cluster then contains embeddings of images of fashion products that are color variants to each other.

However, the supervised model needs manual annotations which may be infeasible to obtain in large real-world industrial datasets (such as those present in our platform). Thus, we now propose a novel self-supervised representation learning model to identify color variants without making use of manual annotations.

### 3.2 Self-Supervised Color Variants Model

As discussed using Figure 2, a random crop of an image may not be the best representative to form contrastive pairs for SSL, at least for our task. Hence, we propose a method that simultaneously considers multiple, fixed, slices/patches of an object to form embeddings. This is illustrated in Figure 4. As our contribution is only specific to the embedding learning component, Figure 4 focuses only on this. As illustrated, the

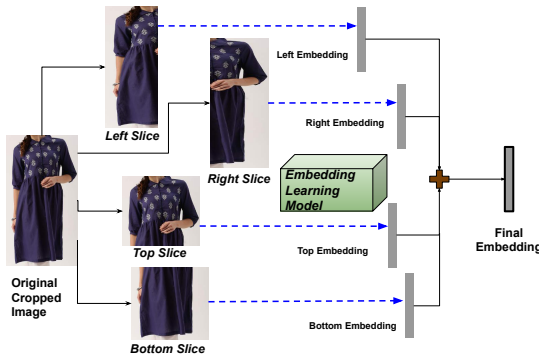


Figure 4: Illustration of our slicing based approach. multiple patches of an object are obtained by performing slices of the image to obtain the left, right, top and bottom views of the object under consideration. We then pass each of these slices through the base encoder of the embedding learning model to obtain four different embeddings, which are then added<sup>1</sup> to obtain the final representation of the object.

We make use of negative pairs in our method because we found the performance of methods that do not make use of negative pairs (eg, SimSiam [Chen and He, 2021], BYOL [Grill *et al.*, 2020]) to be sub-optimal in our use-case. The objective of our method is similar to the commonly used Normalized Temperature-scaled cross entropy (NT-Xent) loss [Chen *et al.*, 2020]. In particular, we make use of two branches for the encoders of our embedding learning model, one for the query and another for the key [Chen *et al.*, 2020; Grill *et al.*, 2020]. In practice, an encoder is a Convolutional Neural Network (CNN) that takes a raw input image and produces an embedding vector. The query encoder is a CNN that obtains embeddings for the anchor images, while the key encoder is a copy of the same CNN that obtains embeddings for the positives and negatives. Gradients are backpropagated only through the query encoder, which is used to obtain the final representations of the inference data.

Following is the objective of our method:

$$\mathcal{L}_q = -\log \frac{\exp(\mathbf{q}\mathbf{k}_q/\tau)}{\sum_{i=0}^K \exp(\mathbf{q}\mathbf{k}_i/\tau)} \quad (1)$$

Here,  $\mathbf{q} = \sum_v \mathbf{q}^{(v)}$ ,  $\mathbf{k}_i = \sum_v \mathbf{k}_i^{(v)}$ ,  $\forall i$ . In (1),  $\mathbf{q}$  and  $\mathbf{k}_i$  respectively denote the *final* embeddings obtained for a query and a key, which are essentially obtained by adding the embeddings obtained from across all the views, as denoted by the superscript  $v$  for  $\mathbf{q}^{(v)}$  and  $\mathbf{k}_i^{(v)}$ . Also,  $\mathbf{k}_q$  represents the positive key corresponding to a query  $\mathbf{q}$ ,  $\tau$  denotes the temperature parameter, whereas  $\exp()$  and  $\log()$  respectively denote the exponential and logarithmic functions.

During our experiments, we observed that simple methods like SimSiam [Chen and He, 2021] do not actually perform too well for our use-case. On the contrary, we found benefits of components such as the momentum encoder, as present in BYOL [Grill *et al.*, 2020] and MOCOv2 [He *et al.*, 2020]. Also, adding an extra memory module in the form of a queue helps in boosting the performance due to comparisons with a large number of negatives. Thus,  $K$  in (1) denotes the size

<sup>1</sup>Rather than concatenating or averaging, we simply add them together to maintain simplicity of the model.

of the memory module. Our method is called as **Patch-Based Contrastive Net (PBCNet)**.

## 4 Experiments

We evaluated the discussed methods on a large (orders of magnitudes of  $10^5$ ) internal collection of challenging real-world industrial images on our Myntra platform (www.myntra.com) that hosts various fashion products. In this section, we report our results on a collection of roughly<sup>2</sup> 0.13 million Kurtas images from our internal database. We used the exact same set to train the supervised (with labeled training data) and self-supervised methods (without labeled training data) for a fair comparison. For inferencing, we used the entire 0.13 million Kurtas images, which are present in the form of different dataset splits (based on brand, gender, MRP). We refer to our 6 dataset splits as Data 1-6. Details of the data and the performance metrics (CGacc for all splits, ARI, FMS and CScore for splits 4-6, a higher value indicates a better performance) are deferred to the supplementary material.

**Methods Compared:** Following are the methods that we have compared for representation learning:

1. **Triplet Loss based Deep Neural Network** [Schroff *et al.*, 2015; Veit *et al.*, 2017]: This is our supervised baseline that is trained using triplet based constraints obtained using the labeled data.
2. **SimSiam** [Chen and He, 2021]: This is a recently proposed State-Of-The-Art (SOTA) visual SSL method that neither uses negative pairs, nor momentum encoder, nor large batches.
3. **BYOL** [Grill *et al.*, 2020]: This is another recently proposed SOTA SSL method that also does not make use of negative pairs, but makes use of batch normalization and momentum encoding.
4. **MOCOv2** [He *et al.*, 2020]: This is a SOTA SSL method that makes use of negative pairs, a momentum encoder, as well as a memory queue.
5. **PBCNet**: This is our proposed novel self-supervised method.

We implemented all the methods in PyTorch. For all the compared methods, we fix a ResNet34 [He *et al.*, 2016] as a base encoder with  $224 \times 224$  image resizing, and train all the models for a fixed number of 30 epochs, for a fair comparison. The number of epochs was fixed based on observations on the supervised model, to avoid overfitting. For the purpose of object detection, we made use of YOLOv2 [Redmon and Farhadi, 2017], and for the task of clustering the embeddings, we made use of the Agglomerative Clustering algorithm with Ward’s method for merging. In all cases, the 512-dimensional embeddings used for clustering are obtained using the avgpool layer of the trained encoder. A margin of 0.2 has been used in the triplet loss for training the supervised model.

### 4.1 Systematic Study of SSL for color variants identification

We now perform a systematic study of the typical aspects associated with SSL, especially for our particular task of color

<sup>2</sup>Company compliance policies prohibit open-sourcing/ revealing exact dataset specifics

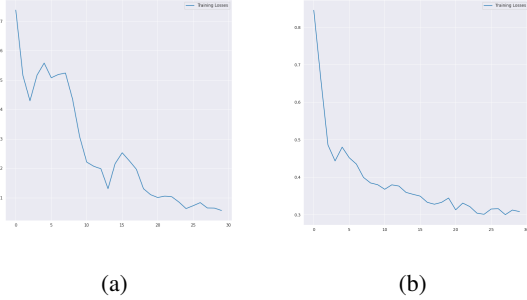


Figure 5: (a) Convergence behaviour of SimSiam\_v0: Validation of the fact that SimSiam actually converges (while avoiding model collapse) with an arbitrary data augmentation. (b) Convergence behaviour of SimSiam\_v1: Considering standard augmentations with random crops leads to a better convergence.

Dataset	Metric	SimSiam_v0		SimSiam_v1	
		(w/o norm)	SimSiam_v0	(w/o norm)	SimSiam_v1
Data 1	CGacc	0.5	0.5	1	0.67
Data 2	CGacc	0.5	<b>0.67</b>	0	<b>0.25</b>
Data 3	CGacc	0	<b>0.4</b>	0	<b>0.33</b>

Table 1: Effect of Embedding Normalization.

variants identification. For this purpose, we make use of a single Table 2, where we provide the comparison of various SSL methods, including ours.

**Convergence behavior with data augmentation for our task:** For illustrating how the convergence behavior of SSL methods changes with respect to a different data augmentation, we pick the SimSiam SSL method for its simplicity and strong claims. We consider two variants of SimSiam: i) SimSiam\_v0: A version of SimSiam, where we used the entire original image as the query, and a color jittered image as the positive, and with a batch size of 12, and ii) SimSiam\_v1: A version of SimSiam with standard SSL [Chen *et al.*, 2020] augmentations (ColorJitter, RandomGrayscale, RandomHorizontalFlip, GaussianBlur and RandomResizedCrop), and a batch size of 12. For all cases, the following architecture has been used for SimSiam: Encoder{ ResNet34  $\rightarrow$  (avgpool)  $\rightarrow$  ProjectorMLP(512 $\rightarrow$ 4096 $\rightarrow$ 123) } $\rightarrow$ PredictorMLP(123 $\rightarrow$ 4096 $\rightarrow$ 123).

Figure 5a shows the convergence behaviour of SimSiam\_v0. It can be seen that SimSiam actually converges with an arbitrary data augmentation, while avoiding a model collapse even without making use of negative pairs. Figure 5b shows the convergence behaviour of SimSiam\_v1. We observed that considering standard augmentations with random crops leads to a better convergence than that of SimSiam\_v0. Thus, for all other self-supervised baselines, i.e., BYOL and MOCOv2 we make use of standard augmentations with random crops. However, we later show that our proposed way of considering multiple patches in PBCNet leads to a better performance.

**Effect of  $l_2$  normalization for our task:** Table 1 shows the effect of performing  $l_2$  normalization on the embeddings obtained using SimSiam. We found that without using any normalization, in some cases (eg, Data 2-3) there are no true color variant groups out of the detected clusters (i.e., zero precision), and hence the performance metrics become zero. Thus, for all our later experiments, we make use of  $l_2$  normalization on the

embeddings as a de facto standard, for all the methods.

**Effect of Batch Size and Momentum Encoding in SSL for our task:** For studying the effect of batch size in SSL for our task, we introduce a third variant of SimSiam, i.e., SimSiam\_v2: This is essentially SimSiam\_v1 with a batch size of 128. We then consider SimSiam\_v1, SimSiam\_v2 and BYOL, where the first makes use of a batch size of 12, while the others make use of batch sizes of 128. We observed that a larger batch size usually leads to a better performance. This is observed from Table 2, by the higher values of performance metrics in the columns for SimSiam\_v2 and BYOL (vs SimSiam\_v1). Additionally, we noted that the momentum encoder used in BYOL causes a further boost in the performance, as observed in its superior performance as compared to SimSiam\_v2 that has the same batch size. It should be noted that except for the momentum encoder, the rest of the architecture and augmentations used in BYOL are exactly the same as in SimSiam. We observed that increasing the batch size in SimSiam does not drastically or consistently improve its performance, something which its authors also noticed [Chen and He, 2021].

**Effect of Memory Queue in SSL for our task:** We also inspect the effect of an extra memory module/queue being used to facilitate the comparisons with a large number of negative examples. In particular, we make use of the MOCOv2 method with the following settings: i) queue size of 5k, ii) temperature parameter of 0.05, iii) a MLP (512 $\rightarrow$ 4096 $\rightarrow$ relu $\rightarrow$ 123) added after the avgpool layer of the ResNet34, iv) SGD for updating the query encoder, with learning rate of 0.001, momentum of 0.9, weight decay of  $1e^{-6}$ , and v) value of 0.999 for  $\theta$  in the momentum update. It is observed from Table 2, by the columns of MOCOv2 and BYOL, that the performance of the former is superior. As BYOL does not use a memory module, but MOCOv2 does, we conclude that using a separate memory module significantly boosts the performance of SSL in our task. Motivated by our observations so far, we choose to employ both momentum encoding and memory module in our proposed PBCNet method.

## 4.2 Comparison of PBCNet against the state-of-the-art

In Table 2, we provide the comparison of our proposed self-supervised method **PBCNet** against various self-supervised state-of-the-art baselines and the supervised baseline across all the datasets. It should be noted that in Table 2, any performance gains for a specific method is due to the intrinsic nature of the same, and not because of a particular hyperparameter setting. This is because we report the *best performance for each method* after adequate tuning of distance threshold (details in supplementary) and other parameters, and not just their default hyperparameters. Following are the configurations that we have used in our **PBCNet** method: i) memory module size of 5k, ii) temperature parameter of 0.05, iii) the FC layer after the avgpool layer of the ResNet34 was removed, iv) SGD for updating the query encoder, with learning rate of 0.001, momentum of 0.9, weight decay of  $1e^{-6}$ , and v) value of 0.999 for  $\theta$  in the momentum update.

We made use of a batch size of 32(= 128/4) as we have to store tensors for each of the 4 slices simultaneously for each mini-batch (we used a batch size of

Dataset	Metric	Supervised	Self-Supervised					PBCNet (Ours)
		Triplet Net	SimSiam_v0	SimSiam_v1	SimSiam_v2	BYOL	MOCov2	
Data 1	CGacc	<b>0.67</b>	0.5	0.67	1	0.5	1	<b>1</b>
Data 2	CGacc	<b>1</b>	0.67	0.25	1	0.75	<b>0.8</b>	0.75
Data 3	CGacc	<b>0.75</b>	0.4	0.33	0	0.5	0.5	<b>0.6</b>
Data 4	CGacc	<b>0.67</b>	0.4	0.5	0.5	0.5	<b>1</b>	0.85
	ARI	<b>0.69</b>	0.09	0.15	0.12	0.27	0.66	<b>0.75</b>
	FMS	<b>0.71</b>	0.15	0.22	0.20	0.30	0.71	<b>0.76</b>
	CScore	<b>0.700</b>	0.110	0.182	0.152	0.281	0.680	<b>0.756</b>
Data 5	CGacc	<b>1</b>	0	0.5	0.33	0.5	1	<b>1</b>
	ARI	<b>1</b>	0	0.09	0.28	0.64	1	<b>1</b>
	FMS	<b>1</b>	0.22	0.30	0.45	0.71	1	<b>1</b>
	CScore	<b>1</b>	0	0.135	0.341	0.674	1	<b>1</b>
Data 6	CGacc	<b>0.83</b>	0.5	0.5	0.8	0.6	1	<b>1</b>
	ARI	<b>0.44</b>	0.07	0.06	0.04	0.20	0.58	<b>0.79</b>
	FMS	<b>0.49</b>	0.12	0.17	0.13	0.24	0.64	<b>0.80</b>
	CScore	<b>0.466</b>	0.089	0.090	0.063	0.214	0.610	<b>0.796</b>

Table 2: Comparison of our proposed method against the supervised and state-of-the-art self-supervised baselines, across all the datasets.



Figure 6: Qualitative comparison of color variants groups obtained using our PBCNet method (left column), MOCov2 (middle column) and the supervised baseline (right column), on *Data 4*.

128 for the other methods). For data augmentation, we first apply a color distortion in the following order: i) ColorJitter( $0.8 * s$ ,  $0.8 * s$ ,  $0.8 * s$ ,  $0.2 * s$ ) with  $s=1$ ,  $p=0.8$ , ii) RandomGrayscale with  $p=0.2$ , iii) GaussianBlur( $(3, 3)$ ,  $(1.0, 2.0)$ ) with  $p=0.5$ . After the color distortion, we apply our slicing technique. For the second image (positive/negative) we apply the same series of transformations.

From Table 2, it is clear that the SimSiam method despite its strong claims of not using any negative pairs, nor momentum encoder nor large batches, performs poorly as compared to our supervised method (shown in bold blue color). The BYOL method which also do not make use of negative pairs, performs better than the SimSiam method in our use case, by virtue of its momentum encoder.

Among all compared SSL baselines, it is the MOCov2 method that performs the best. This is due to the reason of the memory queue that facilitates the comparison with a large number of negative examples. This shows that the importance of considering negative pairs still holds true, especially for challenging use-cases like the one considered in the paper. However, our proposed self-supervised method **PBCNet** clearly outperforms all the baselines. The fact that it outperforms MOCov2 can be attributed to the patch-based slicing used, which is the only different component in our method in comparison to MOCov2 that uses random crop. Another interesting thing that we observed is the fact that despite using much lesser batch size of 32, our method outperforms the baselines. In a way, we were able to extract and leverage more

Method	Clustering	Data 4		Data 5		Data 6	
		ARI	FMS	ARI	FMS	ARI	FMS
PBCNet	Agglo	<b>0.75</b>	<b>0.76</b>	<b>1.00</b>	<b>1.00</b>	<b>0.79</b>	<b>0.80</b>
	DBSCAN	0.66	0.71	1.00	1.00	0.66	0.71
	Affinity	0.30	0.42	0.22	0.41	0.24	0.37
MOCov2	Agglo	<b>0.66</b>	<b>0.71</b>	<b>1.00</b>	<b>1.00</b>	<b>0.58</b>	<b>0.64</b>
	DBSCAN	0.66	0.71	1.00	1.00	0.37	0.40
	Affinity	0.20	0.32	0.04	0.26	0.25	0.41
BYOL	Agglo	<b>0.27</b>	<b>0.30</b>	<b>0.64</b>	<b>0.71</b>	<b>0.20</b>	<b>0.24</b>
	DBSCAN	0.17	0.28	0.64	0.71	0.02	0.24
	Affinity	0.03	0.14	0.28	0.45	0.01	0.11

Table 3: Effect of the clustering technique used.

Dataset	Method	Data 1	Data 2	Data 3	Data 4			Data 5			Data 6		
		CGacc	CGacc	CGacc	CGacc	ARI	FMS	CGacc	ARI	FMS	CGacc	ARI	FMS
PBCNet-horiz	1	1	0.5	0.66	0.65	0.67	1	1	1	1	<b>0.81</b>	<b>0.82</b>	
PBCNet-vert	1	0.6	0.6	<b>1</b>	<b>0.88</b>	<b>0.89</b>	1	1	1	1	0.83	0.48	0.50
PBCNet	1	0.75	<b>0.6</b>	0.85	0.75	0.76	1	1	1	1	0.79	0.80	

Table 4: Effect of Slicing on PBCNet

information by virtue of the slicing (by borrowing information from the other patches simultaneously), even with smaller batches.

We also noticed that the supervised baseline performs quite good in our task, even without any data augmentation pipeline as used in the SSL methods. However, by virtue of data augmentations like color jitter and cropping, which are pretty relevant to the task of color variants identification, stronger SSL methods like MOCov2 and PBCNet are in fact capable of surpassing the performance of the supervised baseline as well, in some cases. Having said that, if we do not have adequate labeled data in the first place, we cannot even use supervised learning. Hence, enabling data augmentations and slicing strategy in the supervised model has not been focused, because the necessity of our approach comes from the issue of addressing the lack of labeled data, and not to improve the performance of supervised learning (which any how is label dependent).

**Effect of Clustering:** In Table 3, we report the performances obtained by varying the clustering algorithm to group embeddings obtained by different SSL methods, on *Data 4-6*. We picked the Agglomerative, DBSCAN and Affinity Propagation clustering techniques that do not require the number of clusters as input parameter (which is difficult to obtain in our use-case). In general, we observed that the Agglomerative clustering technique leads to a better performance in our use-case. Also, for a fixed clustering approach, using embeddings obtained by our PBCNet method usually leads to a better performance.

**Qualitative results:** Sample qualitative comparisons of color variants groups obtained on *Data 4* using our PBCNet method, MOCov2 and the supervised baseline are provided in Figure 6. Each of the rows for a column corresponding to a method represents a detected color variants cluster for the considered method. A row has been marked with a red box if



Figure 7: A few groups obtained on *Data 2* & *3* using MOCOv2 have false positives (shown in red box), while our PBCNet method does not yield such groups.



Figure 8: Trade off between vertical and horizontal slicing.

the entire cluster contains images that are not color variants to each other. A single image is marked with a red box if it is the only incorrect image, while rest of the images are color variants. We observed that our method not only detects clusters with higher precision (which MOCOv2 does as well), but it also has a higher recall, which is comparable to the supervised method. We also make use of a blue box to show a detected color group by our method which contains images that are color variants, but are difficult to be identified at a first glance.

Additionally, Figure 7 shows a few color groups identified in the datasets *Data 2* & *3* using MOCOv2 and our PBCNet. We observed that MOCOv2 detected groups with false positives, while our PBCNet method did not. This could happen because when a random crop is obtained by MOCOv2, it need not necessarily be from a *distinctive* region of an apparel that helps to identify its color variant (eg, in Figure 7, the bent line like pattern separating the colored and black region of the apparels of *Data 2*, and the diamond like shape in the apparels of *Data 3*). We argue that a random crop might have arrived from such a *distinctive* region given that the size of the crop is made larger, etc. But that still leaves things to random chance. On the other hand, our slicing technique being deterministic in nature, *guarantees* that all the regions of an object *would* be captured. We would also like to mention that our slicing approach is agnostic to the fashion apparel type, i.e., the same is easily applicable for any fashion article type (Tops, Shirts, Shoes, Trousers, Track pants, Sweatshirts, etc). In fact, this

is how a human identifies color variants as well, by looking at the article along both horizontal and vertical directions, to identify distinctive patterns. Even humans cannot identify an object if we restrict our vision to only a particular small crop.

**Effect of the slicing:** We also study 2 variants of our PBCNet method: i) PBCNet-horiz (computing an embedding only by considering the top and bottom slices), and ii) PBCNet-vert (computing an embedding using only the left and right slices). The results are shown in Table 4. In *Data 4*, PBCNet-vert performs better than PBCNet-horiz, and in *Data 6*, PBCNet-horiz performs better than PBCNet-vert (significantly). The performance of the two versions is also illustrated in Figure 8. We observed that a single slicing do not work in all scenarios, especially for apparels.

Although the horizontal slicing is quite competitive, it may be beneficial to consider the vertical slices as well. This is observed by the drop in performance of PBCNet-horiz in *Data 3-4* (vs PBCNet). This is because some garments may contain distinguishing patterns that may be better interpreted only by viewing vertically, for example, printed texts (say, *adidas* written vertically), floral patterns etc. In such cases, simply considering horizontal slices may actually split/ disrupt the vertical information. It may also happen that mixing of slicing introduces some form of redundancy, as observed by the occasional drop in the performance of PBCNet when compared to PBCNet-horiz (on *Data 6*) and PBCNet-vert (on *Data 4*). However, on average PBCNet leads to an overall consistent and competitive performance, while avoiding drastically fluctuating improvements or failures. We suggest considering both the directions of slicing, so that they could collectively represent all necessary and distinguishing patterns, and if one slicing misses some important information, the other could compensate for it.

## 5 Conclusions

In this paper, we utilize deep visual Representation Learning to address the problem of identification of color variants (images of objects exactly similar in design, but not color), particularly for fashion products. A supervised triplet loss based deep neural network model for visual Representation Learning has been proposed to identify the color variants. A systematic study of existing state-of-the-art self-supervised methods has been done to solve the proposed problem, while alleviating the need for manual annotations. Also, a novel contrastive loss based self-supervised representation learning method that focuses on parts of an object has been proposed. This is done to make the model better informed of the discriminative regions of an image, in order to identify color variants.

## References

- [Cao *et al.*, 2019] Xuefei Cao, Bor-Chun Chen, and Ser-Nam Lim. Unsupervised deep metric learning via auxiliary rotation loss. *arXiv preprint arXiv:1911.07072*, 2019.
- [Chen and He, 2021] Xinlei Chen and Kaiming He. Exploring simple siamese representation learning. *Proc. of IEEE Conference on Computer Vision and Pattern Recognition (CVPR)*, 2021.
- [Chen *et al.*, 2020] Ting Chen, Simon Kornblith, Mohammad Norouzi, and Geoffrey Hinton. A simple framework for con-

trastive learning of visual representations. In *Proc. of International Conference on Machine Learning (ICML)*, pages 1597–1607. PMLR, 2020.

[Dutta *et al.*, 2020a] Ujjal Kr Dutta, Mehrtash Harandi, and C Chandra Sekhar. Unsupervised metric learning with synthetic examples. In *Proc. of Association for the Advancement of Artificial Intelligence (AAAI)*, 2020.

[Dutta *et al.*, 2020b] Ujjal Kr Dutta, Mehrtash Harandi, and Chellu Chandra Sekhar. Unsupervised deep metric learning via orthogonality based probabilistic loss. *IEEE Transactions on Artificial Intelligence (TAI)*, 1(1):74–84, 2020.

[Grill *et al.*, 2020] Jean-Bastien Grill, Florian Strub, Florent Alché, Corentin Tallec, Pierre H Richemond, Elena Buchatskaya, Carl Doersch, Bernardo Avila Pires, Zhaohan Daniel Guo, Mohammad Gheshlaghi Azar, et al. Bootstrap your own latent: A new approach to self-supervised learning. *arXiv preprint arXiv:2006.07733*, 2020.

[Gu and Ko, 2020] Geonmo Gu and Byungsoo Ko. Symmetrical synthesis for deep metric learning. In *Proc. of Association for the Advancement of Artificial Intelligence (AAAI)*, 2020.

[He *et al.*, 2016] Kaiming He, Xiangyu Zhang, Shaoqing Ren, and Jian Sun. Deep residual learning for image recognition. In *Proc. of IEEE Conference on Computer Vision and Pattern Recognition (CVPR)*, pages 770–778, 2016.

[He *et al.*, 2020] Kaiming He, Haoqi Fan, Yuxin Wu, Saining Xie, and Ross Girshick. Momentum contrast for unsupervised visual representation learning. In *Proc. of IEEE Conference on Computer Vision and Pattern Recognition (CVPR)*, pages 9729–9738, 2020.

[Jagadeesh *et al.*, 2014] Vignesh Jagadeesh, Robinson Piramuthu, Anurag Bhardwaj, Wei Di, and Neel Sundaresan. Large scale visual recommendations from street fashion images. In *Proc. of ACM Special Interest Group on Knowledge Discovery and Data Mining (SIGKDD)*, pages 1925–1934, 2014.

[Jing and Tian, 2020] Longlong Jing and Yingli Tian. Self-supervised visual feature learning with deep neural networks: A survey. *IEEE Transactions on Pattern Analysis and Machine Intelligence (TPAMI)*, 2020.

[Levi *et al.*, 2020] Elad Levi, Tete Xiao, Xiaolong Wang, and Trevor Darrell. Reducing class collapse in metric learning with easy positive sampling. *arXiv preprint arXiv:2006.05162*, 2020.

[Li *et al.*, 2020] Yang Li, Shichao Kan, and Zhihai He. Unsupervised deep metric learning with transformed attention consistency and contrastive clustering loss. In *Proc. of European Conference on Computer Vision (ECCV)*, 2020.

[Redmon and Farhadi, 2017] Joseph Redmon and Ali Farhadi. Yolo9000: better, faster, stronger. In *Proc. of IEEE Conference on Computer Vision and Pattern Recognition (CVPR)*, pages 7263–7271, 2017.

[Schroff *et al.*, 2015] Florian Schroff, Dmitry Kalenichenko, and James Philbin. Facenet: A unified embedding for face recognition and clustering. In *Proc. of IEEE Conference on Computer Vision and Pattern Recognition (CVPR)*, pages 815–823, 2015.

[Sun *et al.*, 2020] Yifan Sun, Changmao Cheng, Yuhan Zhang, Chi Zhang, Liang Zheng, Zhongdao Wang, and Yichen Wei. Circle loss: A unified perspective of pair similarity optimization. In *Proc. of IEEE Conference on Computer Vision and Pattern Recognition (CVPR)*, pages 6398–6407, 2020.

[Veit *et al.*, 2017] Andreas Veit, Serge Belongie, and Theofanis Karalietos. Conditional similarity networks. In *Proc. of IEEE Conference on Computer Vision and Pattern Recognition (CVPR)*, pages 830–838, 2017.

[Wang *et al.*, 2018] Guanshuo Wang, Yufeng Yuan, Xiong Chen, Jiwei Li, and Xi Zhou. Learning discriminative features with multiple granularities for person re-identification. In *Proc. of ACM International Conference on Multimedia (ACMMM)*, pages 274–282, 2018.

## 6 Supplementary: Additional Details and Results (omitted from the main text due to space constraints)

We evaluated the discussed methods on a large (orders of magnitudes of  $10^5$ ) internal collection of challenging real-world industrial images on our Myntra platform ([www.myntra.com](http://www.myntra.com)) that hosts various fashion products. In this section, we report our results on a collection of roughly<sup>3</sup> 0.13 million Kurtas images from our internal database. A disjoint set of 6k images were manually annotated by our in-house team to provide class labels indicating their color variants information. This labeled data was used to form triplets to train the supervised triplet loss based color variants model. We also used the exact same set to train the self-supervised methods for a fair comparison. For inferencing, we used the entire 0.13 million Kurtas images, which are present in the form of different dataset splits (based on brand, gender, MRP). We refer to our 6 dataset splits as Data 1-6. Table 5 provides details of the datasets used to compare the methods, along with their meta-data on our platform. It should be noted that the datasets *Data 1-3* do not have manual annotations available for them, whereas the remaining three have been annotated by the taggers.

Dataset	Article_Type	Gender	Brand	MRP	Ground Truth Available
Data 1	Kurtas	Women	STREET 9	1899	No
Data 2	Kurtas	Women	STREET 9	1399	No
Data 3	Kurtas	Women	STREET 9	1499	No
Data 4	Kurtas	Women	all about you	1699	Yes
Data 5	Kurtas	Women	all about you	2499	Yes
Data 6	Kurtas	Women	all about you	2199	Yes

Table 5: Details of datasets used to compare the methods.

Dataset	Config	Sup	S0	S1	S2	B	M	PB
Data 1	t	1	0.07	0.3	0.3	0.5	0.7	0.8
	nCG	2	1	2	1	1	2	2
	nDG	3	2	3	1	2	2	2
Data 2	t	0.87	0.07	0.15	0.2	0.5	0.8	0.8
	nCG	4	2	1	2	3	4	3
	nDG	4	3	4	2	4	5	4
Data 3	t	0.87	0.2	0.24	0.3	0.5	0.8	0.8
	nCG	3	2	2	0	1	3	3
	nDG	4	5	6	5	7	2	6
Data 4	t	0.8	0.1	0.1	0.5	0.5	0.6	0.8
	nCG	4	2	1	3	3	3	6
	nDG	6	5	2	6	6	3	7
Data 5	t	0.9	0.3	0.6	0.6	0.7	0.7	0.8
	nCG	1	0	1	1	1	1	1
	nDG	1	1	2	3	2	1	1
Data 6	t	0.95	0.07	0.8	0.8	0.6	0.8	0.9
	nCG	5	2	2	4	3	6	7
	nDG	6	4	4	5	5	6	7

Table 6: Distance thresholds in Agglomerative clustering used to produce the *best* results (for each method) across all the datasets, along with the number of *detected* and *correct* color groups. NOTE that we have used the following notations: Config: Configuration, t:threshold, nCG:n.correct\_gps, nDG:n.detected\_gps, Sup:Supervised, S0:SimSiam\_v0, S1:SimSiam\_v1, S2:SimSiam\_v2, B:BYOL, M:MOCOv2, and PB:PBCNet.

<sup>3</sup>Company compliance policies prohibit open-sourcing/ revealing exact dataset specifics

SimSiam.v0					SimSiam.v1					SimSiam.v2				
Method	dist_threshold	CGacc	ARI	FMS	Method	dist_threshold	CGacc	ARI	FMS	Method	dist_threshold	CGacc	ARI	FMS
Data 1	0.07	0.5			Data 1	0.2	1			Data 1	0.3	1		
	0.1	0.33				0.3	0.67				0.5	0.5		
	0.2	0.33				0.4	0.5				0.6	0.5		
	0.07	0.67				0.5	0.67				0.2	1		
	0.1	0.4				0.15	0.25				0.3	0.4		
	0.2	0.25				0.2	0.2				0.4	0.5		
Data 2	0.07	0			Data 2	0.1	0			Data 2	0.2	0		
	0.1	0				0.2	0.2				0.3	0.4		
	0.2	0.4				0.3	0.2				0.4	0.5		
Data 3	0.07	0			Data 3	0.1	0			Data 3	0.2	0		
	0.1	0				0.23 to 0.25	0.33				0.3	0		
Data 4	0.1	0.4	0.09	0.15	Data 4	0.1	0.5	0.15	0.22	Data 4	0.3	0.33	0.14	0.18
	0.3	0				0.00	0.22				0.3	0.5		
Data 5	0.07	0.5	0.07	0.12	Data 5	0.4	0.16	0.09	0.30	Data 5	0.6	0.33	0.28	0.45
Data 6	0.1	0.4	0.01	0.08	Data 6	0.6	0	0.05	0.14	Data 6	1.1	0.5	0.09	0.30
					Data 4	0.2	0.14	0.03	0.08	Data 5	0.6	0.33	0.02	0.09
					Data 5	0.6	0.5	0.09	0.30	Data 6	0.8	0.8	0.04	0.13
					Data 6	0.4	0.5	0.06	0.17	Data 6	0.9	0.75	0.01	0.11
BYOL					MOCOv2					PBCNet				
Method	dist_threshold	CGacc	ARI	FMS	Method	dist_threshold	CGacc	ARI	FMS	Method	dist_threshold	CGacc	ARI	FMS
Data 1	0.5	0.5			Data 1	0.6	1			Data 1	0.6	1		
	0.7	0.5				0.7	1				0.7	1		
	1.1	0.33				0.8	0.67				0.8	1		
Data 2	0.5	0.75			Data 2	0.9	0.5			Data 2	0.9	0.67		
	0.7	0.6				0.6	0				0.9	0.5		
	0.9	0.6				0.7	1				1	1		
Data 3	0.5	0.5			Data 3	0.8	0.8			Data 3	0.8	0.75		
	0.55	0.33				0.9	0.67				0.9	0.67		
	0.6	0.25				0.6	0.5				0.9	0.42		
Data 4	0.7	0.33	0.15	0.22	Data 4	0.6	0.5	0.17	0.32	Data 4	0.6	0.5	0.32	0.45
	0.3	0.5				0.7	0.5				0.7	0.33		
	0.45	0.33				0.8	0.5				0.8	0.6		
Data 5	0.5	0.5	0.22	0.26	Data 5	0.6	1	0.66	0.71	Data 5	0.9	0.42	0.75	0.76
	0.7	0.5				0.7	0.57				0.6	0.67		
	0.8	0.33				0.8	0.67				0.8	0.37		
Data 6	0.55	0.67	0.12	0.16	Data 6	0.9	0.6	1.00	1.00	Data 6	0.9	0.85	0.65	0.68
	0.6	0.6				0.7	1				0.6	0.5		
						0.8	0.5				0.8	0.5		
					Data 5	0.6	1	0.39	0.50	Data 5	0.6	1	1.00	1.00
					Data 6	0.7	0.67	0.34	0.37	Data 6	0.7	1	1.00	1.00
					Data 6	0.8	1	0.58	0.64	Data 6	0.8	1	1.00	1.00
					Data 6	0.9	0.85	0.56	0.65	Data 6	0.9	0.85	0.64	0.71
										Data 6	0.6	1	0.39	0.50
										Data 6	0.7	1	0.66	0.71
										Data 6	0.8	1	0.70	0.72
										Data 6	0.9	1	0.79	0.80
										Data 6	1	1	0.47	0.53

Table 7: Varying values of performance metrics against distance thresholds. For a method, only those thresholds are reported against a dataset, using which Agglomerative Clustering produces non-zero performance metrics, thus indicating a meaningful clustering.

**Performance metrics used:** To evaluate the methods, we made use of the following performance metrics (CGacc and CScore are defined by us for our use-case):

1. **Color Group Accuracy (CGacc):** It refers to the ratio of the number of *correct color groups* to that of the number of *detected color groups*. Here, *detected color groups* are the clusters identified by the clustering algorithm that have a size of at least two. A *correct color group* is a cluster among the *detected color groups*, which contains at least half of its examples which are actually color variants to each other (while implementing we take a floor function). It should be noted that this performance metric has a direct business relevance due to the fact that it reflects the *precision*. Also, it is computed by our in-house catalog team by performing manual Quality Check (QC).
2. **Adjusted Random Index (ARI):** Let  $s$  (and  $d$ , respectively) be the number of pairs of elements that are in the same (and different, respectively) set in the ground truth class assignment, and in the same (and different, respectively) set in the clustering. Then, the (unadjusted) Random Index is computed as:  $RI = \frac{s+d}{N C_2}$ , where  $N$  is the number of elements clustered. The Adjusted RI (ARI) is then computed as:  $ARI = \frac{RI - \mathbb{E}[RI]}{\max(RI) - \mathbb{E}[RI]}$ . ARI ensures that a random label assignment will get a value close to zero (which RI does not).
3. **Fowlkes-Mallows Score (FMS):** It is computed as:  $FMS = \frac{TP}{\sqrt{(TP+FP)(TP+FN)}}$ , where  $TP$  is the num-

ber of pairs that belong to the same clusters in both the ground truth, as well as the predicted cluster labels,  $FP$  is the number of pairs that belong to the same clusters in the ground truth, but not in the predicted cluster labels, and  $FN$  is the number of pairs that belong in the same clusters in the predicted cluster labels, but not in the ground truth.

4. **Clustering Score (CScore):** It is computed as:  $CScore = \frac{2 \cdot ARI \cdot FMS}{ARI + FMS}$ .

It should be noted that while we use CGacc to compare the methods for all the datasets (*Data 1-6*), the remaining metrics are reported only for the datasets *Data 4-6*, where we have the ground-truth labels. Also, all the performance metrics take values in the range  $[0, 1]$ , where a higher value indicates a better performance.

Also, for each method, the distance threshold used to obtain the results, and the corresponding number of *detected* as well as the number of *correct* groups obtained, are reported in Table 6. From Table 6, we observed that our method is capable of detecting more number of color groups with a usually higher precision, when compared to its competitors.

In Table 7, we report the performance of all the compared self-supervised methods (including ours) on all the datasets, with respect to the different metrics against varying values of the distance threshold used in the Agglomerative clustering.